

Stochastic modelling of microstructures for virtual material design

Claudia Redenbach^{1*}

Micro Abstract

Macroscopic properties of materials, e.g. the permeability of a filter or the mechanical strength of a fiber composite, are highly influenced by the microstructure. Models from stochastic geometry are valuable tools for studying these relations as they allow for the generation of virtual microstructures with controlled characteristics. The talk presents models for different material classes and explains how to fit the models based on geometric characteristics estimated from 3D image data.

¹Mathematics Department, University of Kaiserslautern, Kaiserslautern, Germany

*Corresponding author: redenbach@mathematik.uni-kl.de

Introduction

A key element in the design of modern high performance materials is the understanding of the influence of the material's microstructure geometry on its macroscopic properties. Quantitative analysis of 3D image data provides valuable information on geometric characteristics such as distributions of cell or particle sizes, the specific surface area or the orientation distribution of fibres in composite materials. In a second step, fitting a stochastic model to the observed characteristics allows to modify the microstructure by generating model realizations with altered parameters, e.g. higher fibre content, different fibre cross sections or variations in the fibre orientation distribution. Simulation of macroscopic properties in these 'virtual samples' then helps to predict how certain changes of the microstructure will influence the performance of the material. These findings can then be used to optimize materials for certain applications.

A schematic representation of the cycle of virtual material design is given in Figure 1.

1 Stochastic geometry models

Random closed sets from stochastic geometry provide the framework for defining models for the microscopically heterogeneous geometric microstructure of materials. In the following, we briefly introduce some basic model classes. For rigorous definitions we refer to the textbooks [2, 9].

1.1 Point processes

Point processes are a key ingredient of many stochastic geometry models. Briefly speaking, a point process is a collection of random locations in space. It is called stationary if its distribution is invariant under translations. If the distribution is invariant w.r.t. rotations, the process is called isotropic.

One of the main characteristics of a point process is the intensity measure Λ . For a Borel set B , $\Lambda(B)$ is the expected number of points in B . For stationary point processes, we have $\Lambda(B) = \lambda V(B)$, where $V(B)$ is the volume of B and the constant $\lambda > 0$, the intensity of the point process, is the expected number of points in a unit volume.

The most important point process model is the Poisson process which is used as the reference model for 'complete spatial randomness', i.e. no interaction between the points. The name

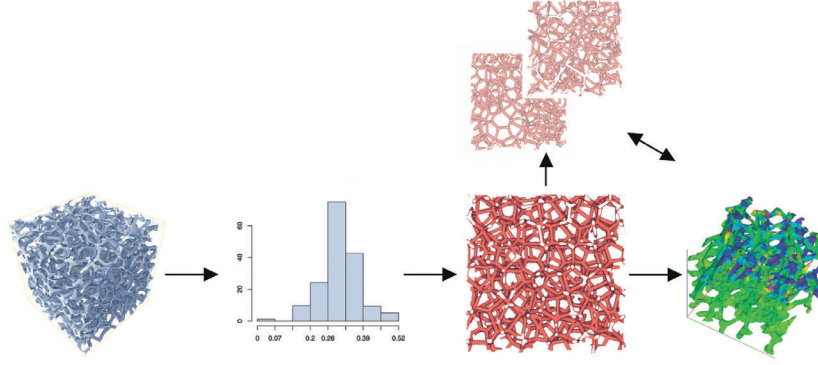


Figure 1. Sketch of virtual material design based on stochastic microstructure modelling: observe a real microstructure through image data (grey), estimate geometric characteristics (histogram), fit a stochastic geometry model (red), simulate materials properties of interest (blue-to-red scale). Generate altered microstructures by modification of model parameters (pale red) and investigate the influence on the simulated properties. Repeat until satisfactory performance is obtained.

Poisson process comes from the fact that the number of points in a bounded set B follows a Poisson distribution with parameter $\Lambda(B)$. There is a variety of additional models which allow for the modelling of interaction (repulsion or attraction/clustering) between the points. The statistical analysis of random point patterns, various models, and methods for parameter estimation are discussed in [1, 4].

1.2 Particle processes

In a more general setting, we can consider point processes whose points are no longer locations but random compact sets in \mathbb{R}^d , e.g. balls, cylinders or polytopes. Such processes are called particle processes. A stationary particle process can also be interpreted as marked point process by splitting up the particles into centre locations $x \in \mathbb{R}^d$ and compact sets C having their centre in the origin. In this case, the intensity measure can be written as $\Lambda = \Lambda_0 \otimes \mathbb{Q}$ where Λ_0 is the intensity measure of the point process of centre locations and \mathbb{Q} is the distribution of the typical particle which determines the particle shape.

One important example is the Boolean model where centre points form a Poisson process and particle shapes are drawn independently and identically distributed from the distribution \mathbb{Q} independently of the locations. Consequently, particles can overlap in this model. In many situations, systems of non-overlapping (or hard) particles are of interest. Such systems can be generated using the Random Sequential Adsorption (RSA) approach. This algorithm is based on sequentially adding particles to the observation window such that overlaps are avoided. To achieve higher packing densities, collective rearrangement algorithms such as the force biased algorithm [5] can be applied. For examples see Figure 2.

1.3 Random tessellations

Random tessellations are special particle processes where the particles form a division of \mathbb{R}^d into bounded cells whose interiors do not intersect. Maybe the most well-known model is the Voronoi tessellation which is defined as follows. Let ϕ be a locally finite set of points in \mathbb{R}^d , e.g. a realisation of a point process Φ . Then the Voronoi cell of $x \in \phi$ is defined as

$$C(x) = \{z \in \mathbb{R}^d : \|x - z\| \leq \|y - z\| \text{ for all } y \in \phi\}, \quad (1)$$

i.e. it consists of all points in \mathbb{R}^d having x as nearest neighbour in ϕ .

The Laguerre tessellation is a weighted generalization of the Voronoi model. To each point $x \in \phi$ we assign a positive weight $r > 0$ such that the pair (x, r) can be interpreted as a sphere with

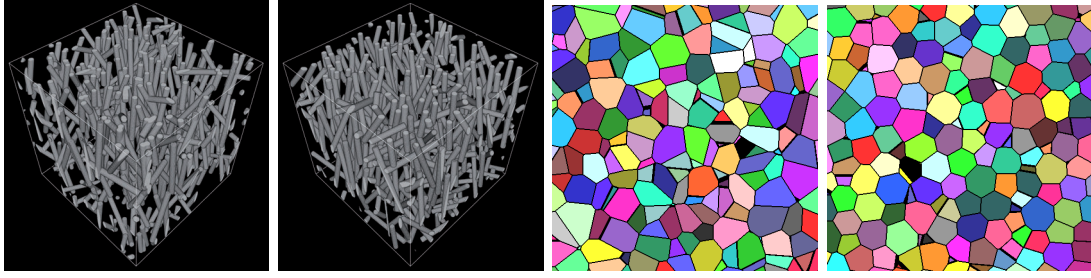


Figure 2. From left to right: Fibre systems generated by a Boolean model (overlapping fibres) and an RSA process (non-overlapping fibres). 2D sections of a Poisson Voronoi tessellation and a Laguerre tessellation generated by a dense packing of balls. Note the differences in cell shape.

radius r centred in x . The Laguerre cell of (x, r) is

$$C(x, r) = \{z \in \mathbb{R}^d : \|x - z\|^2 - r^2 \leq \|y - z\|^2 - s^2 \text{ for all } (y, s) \in \phi\}. \quad (2)$$

Some examples are shown in Figure 2. As in the case of more general particle processes, model fitting is based on observing geometric characteristics of the typical cell of the tessellation, see [7].

2 Geometric characterisation and parameter estimation

To determine the distribution \mathbb{Q} of the typical particle of a particle process, geometric characteristics for the size, orientation and topology of the particles can be considered. A basic set of characteristics are the intrinsic volumes. In \mathbb{R}^3 , these are four characteristics, namely – up to constant factors – the volume $V = V_3$, the surface area $S = 2V_2$, the integral of mean curvature $M = \pi V_1$, and the Euler number $\chi = V_0$, see e. g. [2]. For convex and compact sets, the integral of mean curvature is up to a constant the mean width $M = 2\pi\bar{b}$ – a measure for the particle diameter defined as the distance of two parallel planes enclosing the particle, averaged w.r.t. rotation. Intrinsic volumes can efficiently be estimated from binary image data using the approach described in [6].

Besides the analysis of separate particles, also analysing their union, e.g. the fibre system in a glass fibre material, may provide valuable information. In this case, the *densities of the intrinsic volumes* are considered. In practice, they are computed as

$$V_{V,k}(\Xi) = \frac{V_k(\Xi \cap W)}{V_d(W)}, \quad k = 0, \dots, d, \quad (3)$$

where W is the observation window and Ξ is the random closed set of interest.

In \mathbb{R}^3 the densities of the intrinsic volumes are the volume density $V_V = V_{V,3}$, the surface area density (or specific surface area) $S_V = 2V_{V,2}$, the density of the integral of mean curvature $M_V = \pi V_{V,1}$, and the density of the Euler number $\chi_V = V_{V,0}$.

For a stationary Boolean model, the mean intrinsic volumes of the typical particle and the intensity λ can be computed from the intrinsic volume densities using the Miles formulas [9]. For systems of non-overlapping particles, one has

$$V_V = \lambda\bar{V}, S_V = \lambda\bar{S}, M_V = 2\pi\lambda\bar{b}, \chi_V = \lambda, \quad (4)$$

where \bar{V} , \bar{S} , and \bar{b} are the means of the volume, surface area, and mean width of the typical particle, respectively.

For fibre systems, the fibre orientation distribution is of additional interest. There are several approaches for determining the distribution of the local fibre orientation, i.e. the orientation in the typical fibre point, see [10].

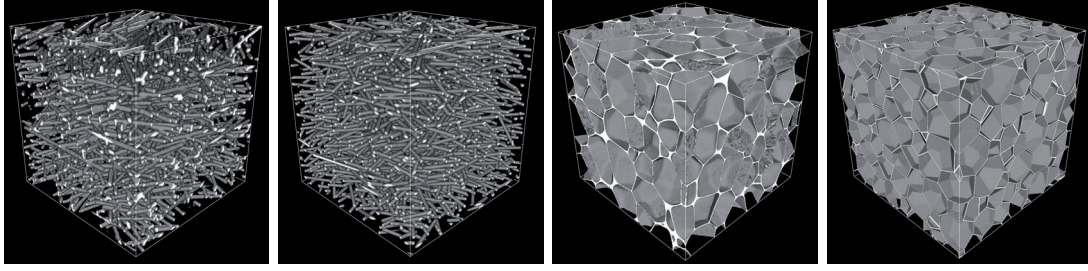


Figure 3. Volume renderings of CT images of real materials and the corresponding models. Left: A glass fibre composite and the fitted RSA model. The visualised volume is 300^3 pixels which corresponds to a cube of edge length 0.765 mm. Right: A closed PMI foam and the fitted Laguerre tessellation. The visualised volume is 600^3 pixels which corresponds to a cube of edge length 1.6 mm.

3 Application examples

In the following, we will discuss two application examples: modelling of a glass fibre reinforced polymer by a system of random cylinders and modelling of a closed cell polymer foam by a random Laguerre tessellation. Details on the materials and the model fit can be found in [8].

3.1 Fiber composite

As a first example we consider a sample of glass fibre reinforced composite with relatively low fibre content (15 % by weight, 7.3 % by volume). Model fitting is based on a μ CT image of the material consisting of $1660 \times 1660 \times 1211$ pixels. The pixel edge length is $2.5 \mu\text{m}$.

The image was binarised to obtain a volume fraction of $V_V = 7.3\%$ which is the nominal value provided by the producer of the material. The fibre length distribution was modelled by a lognormal distribution with a mean of $250 \mu\text{m}$ and a standard deviation of $189 \mu\text{m}$. Estimates for the (constant) fibre radius R and the intensity λ are obtained from the Equations (4) as $\hat{R} = 6.1 \mu\text{m}$ and $\hat{\lambda} = 2465.1/\text{mm}^3$. The fibre direction distribution is modelled by the parametric distribution model presented in [3]. The concentration parameter is chosen as $\beta = 6$ which yields a girdle distribution, i.e. a distribution concentrated in a plane. The normal vector of this plane is estimated as $(-0.017, 0.0033, 0.9999)^T$ resulting in fibres oriented along the xy -plane. Fibers are placed in the volume using the RSA approach introduced above. Visualisations of the original material and a model realisation are shown in Figure 3 (left).

3.2 Closed foam

Our second example is a sample of a Rohacell closed cell polymer foam. We analyse a μ CT image of size $1200 \times 1100 \times 1300$ pixels with a pixel edge length of $2.7 \mu\text{m}$. As cell walls in this material are thin compared to the cell size, not all walls are sufficiently resolved in the CT image. This results in some holes in cell walls in the segmented image (see Figure 3). By application of the cell reconstruction method based on the watershed transform presented in [6], the cells can be separated and analysed. The estimated cell intensity in the sample is $\hat{\lambda} = 47.61/\text{mm}^3$. The cell system is modelled by a Laguerre tessellation generated by a dense packing of spheres with gamma distributed volumes. For model fitting, moments of the distribution of cell volume, surface area, mean width, and number of facets are considered, see [7] for details. Visualisations of the original material and a model realisation are shown in Figure 3 (right).

References

- [1] A. Baddeley, E. Rubak, and R. Turner. *Spatial Point Patterns: Methodology and Applications with R*. Chapman and Hall, CRC Press, Boca Raton, 2015.

- [2] S. Chiu, D. Stoyan, W. S. Kendall, and J. Mecke. *Stochastic Geometry and Its Applications*. Wiley, Chichester, third edition, 2013.
- [3] J. Franke, C. Redenbach, and N. Zhang. On a mixture model for directional data on the sphere. *Scandinavian Journal of Statistics*, 43(1):139–155, 2016.
- [4] J. Illian, A. Penttinen, H. Stoyan, and D. Stoyan. *Statistical Analysis and Modelling of Spatial Point Patterns*. John Wiley & Sons, Chichester, 2008.
- [5] J. Mościński, M. Bargieł, Z. A. Rycerz, and P. W. M. Jacobs. The force-biased algorithm for the irregular close packing of equal hard spheres. *Molecular Simulation*, 3(4):201–212, 1989.
- [6] J. Ohser and K. Schladitz. *3d Images of Materials Structures – Processing and Analysis*. Wiley VCH, Weinheim, 2009.
- [7] C. Redenbach. Microstructure models for cellular materials. *Computational Materials Science*, 44(4):1397–1407, 2009.
- [8] C. Redenbach, K. Schladitz, I. Vecchio, and O. Wirjadi. Image analysis for microstructures based on stochastic models. *GAMM-Mitteilungen*, 37(2):281–305, 2014.
- [9] R. Schneider and W. Weil. *Stochastic and Integral Geometry*. Probability and Its Applications. Springer, Heidelberg, 2008.
- [10] O. Wirjadi, K. Schladitz, P. Easwaran, and J. Ohser. Estimating fibre direction distributions of reinforced composites from tomographic images. *Image Analysis & Stereology*, 35(3):167–179, 2016.